20th IMEKO TC10 Conference
"Measurement for Diagnostics, Optimization and Control to Support Competitiveness and Innovation"
Lisbon, Portugal, September 28–29, 2026

Data-driven feedforward iterative tuning for MLPM with position-dependent nonlinearities

Qin Guangyi[1], Chen Hao[1], Song Shuo[1], Dong Yue[1], Li Li[1]

[1] *Center of Ultra-precision Optoelectronic Instrument Engineering, Harbin Institute of Technology, Harbin, China, 21b901033@stu.hit.edu.cn, eiddlechen123@163.com, 23b901017@stu.hit.edu.cn, ydonghit@hit.edu.cn, hitlili@hit.edu.cn*

***Abstract* – To address spatial nonlinear position-dependent hybrid additive and multiplicative disturbances in Magnetically Levitated Planar Motor (MLPM) caused by decoupling mismatch, this paper proposes a data-driven position-dependent nonlinear feedforward iterative tuning method. Unlike conventional polynomial feedforward approaches, the proposed rational feedforward controller uses its numerator to compensate additive disturbances and the reference trajectory, and its denominator to handle multiplicative disturbances. Comparative experiments show that the proposed method well compensates both types of disturbances over the full stroke, effectively overcoming the performance degradation of conventional feedforward methods, and significantly improving global dynamic tracking accuracy.**

Keywords* – *MLPM, iterative feedforward tuning, position-dependent disturbances.

I. INTRODUCTION

Magnetically levitated planar motors (MLPMs) are widely used in high-precision positioning systems such as lithography machines, scanning probes, and microscopes [1]. As the semiconductor industry advances toward smaller nodes, these applications increasingly demand MLPMs to achieve micrometer-level tracking accuracy and extreme dynamic responses. MLPMs enable multiple degree-of-freedom (DOF) motion without stacked structures and can operate in vacuum environments [2], avoiding friction, contamination, and error accumulation. However, practical systems still suffer from multi-DOF coupling, position-dependent modelling errors, and inaccurate current allocation, which significantly degrade performance [3, 4]. These practical challenges primarily stem from the complex spatial harmonics of the magnetic fields and mechanical installation errors, which cause the dynamic characteristics of the system to suffer from complex nonlinearities across the operational workspace.

Due to position-dependent gains and gravity-compensation-induced disturbances, MLPMs cannot be accurately modelled as linear time-invariant (LTI) systems [5]. Conventional feedforward control typically uses constant gains based on velocity and acceleration [6], which is inadequate when strong spatial variation exists, since the required compensation changes with position. Consequently, applying a fixed-gain feedforward controller often results in over-compensation or under-compensation depending on the mover's instantaneous location. This mismatch inevitably destroys the global tracking accuracy during operations.

To improve the tracking performance, data-driven methods have been widely studied. Iterative learning control (ILC) is effective for repetitive disturbances [7], but its learning signal is strictly trajectory-dependent, leading to poor generalization when the reference changes [8]. Parameterized feedforward iterative tuning methods extend this idea by optimizing controller parameters for different trajectories [9, 10], but most approaches still rely on constant-gain structures derived from the LTI system assumptions. Without explicitly embedding position dependence, achieving uniformly good performance over the full workspace remains difficult [11]. Therefore, designing a nonlinear decoupling strategy that combines the learning capability of ILC with the generalization ability of parameterized feedforward control remains an open challenge.

This paper proposes a data-driven position-dependent nonlinear feedforward iterative tuning method for MLPMs. Unlike polynomial feedforward approaches, the proposed rational feedforward controller uses its numerator to compensate the reference trajectory and additive disturbances, and its denominator to handle multiplicative disturbances. The model parameters are directly learned from the servo error in an iterative manner to compensate spatial nonlinearities.

The remainder of this paper is organized as follows. Section II introduces the MLPM system and control architecture, and describes its position-dependent nonlinear characteristics. Section III presents the proposed method in brief. Section IV provides the experimental setup and comparative results. Section V concludes the paper.

II.PROBLEM FORMULATION

A. *MLPM control system*

As shown in Fig. 1, the MLPM mainly consists of a stator with a two-dimensional Halbach array and a mover with a coil array. The multi- DOF motion of the mover is achieved by independently controlling the currents in each coil, forming a typical multi-input-multi-output (MIMO) system. High-precision control of MLPMs usually relies on model-based decoupling strategies, aiming to decompose the coupled six-DOF dynamics into six independent single-input-single-output (SISO) systems.

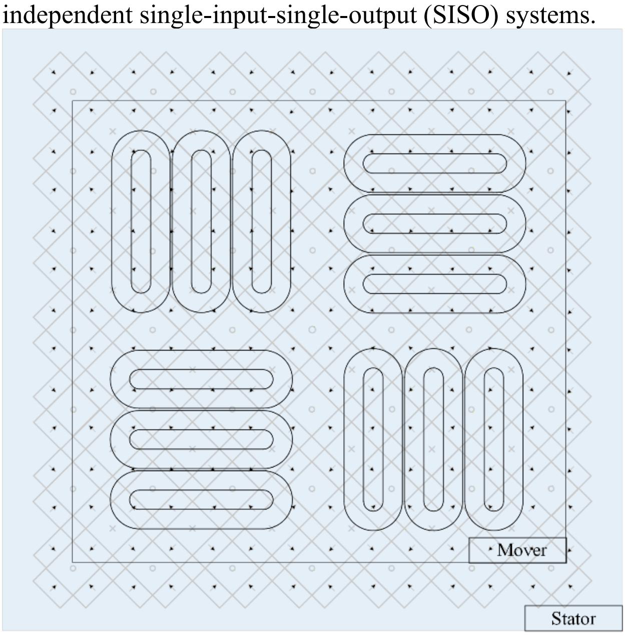

Fig. 1. Simplified structure of the MLPM.

The 6-DOF closed-loop control framework of the MLPM is illustrated in Fig. 2. $\mathbf{r} = [r_x, r_y, r_z, r_{\theta x}, r_{\theta y}, r_{\theta z}]^T$ represents the reference trajectory, $\mathbf{p} = [x, y, z, \theta_x, \theta_y, \theta_z]^T$ is the measured position, and $\mathbf{e} = \mathbf{r} - \mathbf{p}$ is the tracking error . Based on the error signal, the multi-axis feedback controller $\mathbf{C}_{\text{fb}}(s)$ generates the logical control effort $\mathbf{u}_{\text{fb}}$. The logical control effort is defined as

$$\mathbf{u}_{\text{fb}} = \left[u_{\text{fb},x}, u_{\text{fb},y}, u_{\text{fb},z}, u_{\text{fb},\theta_x}, u_{\text{fb},\theta_y}, u_{\text{fb},\theta_z} \right]^T$$

The feedback controller is written as

$$\mathbf{C}_{\text{fb}}(s) = \text{diag}\{C_{\text{fb},k}(s)\}, \quad k \in \{x, y, z, \theta_x, \theta_y, \theta_z\}$$

where each diagonal element denotes the SISO feedback controller designed for the corresponding DOF. To actuate the mover, a position-dependent current allocation matrix $\mathbf{D}(\mathbf{p}) \in \mathbb{R}^{12\times 6}$ maps the logical command $\mathbf{u}_{\text{fb}}$ to the actual coil current $\mathbf{i} \in \mathbb{R}^{12\times 1}$. Subsequently, the physical actuation matrix $\mathbf{M}(\mathbf{p}) \in \mathbb{R}^{6\times 12}$ maps these currents to the actual forces and torques $\mathbf{f}$ generated on the mover, where $\mathbf{f} = \left[f_x, f_y, f_z, \tau_x, \tau_y, \tau_z \right]^T$. The plant dynamics are represented by $\mathbf{P}(s) \in \mathbb{R}^{6\times 6}$, which maps the generated force and torque vector $\mathbf{f}$ to the measured position vector $\mathbf{p}$. Under the ideal decoupling assumption, $\mathbf{P}(s)$ can be expressed as

$$\mathbf{P}(s) = \text{diag}\left\{ P_x(s), P_y(s), P_z(s), P_{\theta_x}(s), P_{\theta_y}(s), P_{\theta_z}(s) \right\}$$

where each diagonal element represents the equivalent single-DOF dynamics from the corresponding force or torque input to the corresponding position or angular displacement output. Ideally, the overall closed-loop force generation aims to achieve perfect decoupling, satisfying $\mathbf{f} = \mathbf{M}(\mathbf{p})\mathbf{D}(\mathbf{p})\mathbf{u}_{\text{fb}} = \mathbf{u}_{\text{fb}}$.

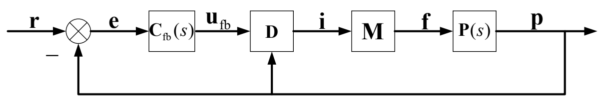

Fig. 2. 6-DOF system control block diagram

B. *Decoupling mismatch & spatial nonlinearities*

Define the coupling matrix as

$$\mathbf{H}(\mathbf{p}) = \mathbf{M}(\mathbf{p})\mathbf{D}(\mathbf{p}) = \left[H_{mn}(\mathbf{p}) \right]_{6\times 6}, \quad m, n \in \{x, y, z, \theta_x, \theta_y, \theta_z\}$$

The diagonal elements $H_{mm}(\mathbf{p})$ describe the effective force or torque gains of the corresponding DOFs, whereas the off-diagonal elements $H_{mn}(\mathbf{p}), m \neq n$, describe the cross-axis coupling from the n-th logical input to the m-th force or torque output. Ideally, if the allocation matrix perfectly matches the true actuation system, then $\mathbf{H}(\mathbf{p}) = \mathbf{I}_{6\times 6}$, yielding $\mathbf{f}(t) = \mathbf{I}_{6\times 6}\mathbf{u}_{\text{fb}}(t)$.

The electromagnetic design of individual coils is originally intended to generate decoupled forces specifically along the horizontal (X or Y) and vertical (Z) axes for propulsion and levitation, respectively. However, due to higher-order magnetic harmonics, manufacturing tolerances, and inherent simplifications in the coil modelling, the actual actuation matrix exhibits strong position dependence, leading to that $\mathbf{H}(\mathbf{p}) \neq \mathbf{I}_{6\times 6}$. Consequently, current inputs originally mapped for specific horizontal or vertical directions inevitably generate parasitic forces and torques in unintended degrees of freedom, giving rise to the cross-axis coupling effect. For example, taking the X-axis as a representative case, the actual force generated along this axis can be expressed as:

$$f_x(t) = H_{xx}(\mathbf{p})u_{\text{fb},x}(t) + \sum_{j\neq x} H_{xj}(\mathbf{p})u_{\text{fb},j}(t) \tag{1}$$

This mismatch introduces significant nonlinear disturbances, which can be categorized as follows:

Position-dependent multiplicative disturbance: Associated with the diagonal term $H_{xx}(\mathbf{p})$. The effective force gain is no longer constant but varies with position, resulting in nonlinear variations in the forward-loop gain.

Position-dependent additive disturbance: Associated with the off-diagonal terms. In active magnetic levitation systems, a large static force command ($u_{\text{fb},z} \approx mg$) is required along the Z-axis to maintain levitation. This command couples into horizontal axes (e.g., X-axis) via $H_{xz}(\mathbf{p})$, producing parasitic forces:

$$f_{\text{add},x}(t) \approx H_{xz}(\mathbf{p}(t))u_{\text{fb},z}(t) \tag{2}$$

Since $H_{xx}(\mathbf{p})$ and $H_{xz}(\mathbf{p})$ vary significantly with the mover position, the resulting multiplicative and additive disturbances cannot be effectively compensated by conventional position-independent feedforward controllers. Moreover, these two disturbance components exhibit fundamentally different characteristics. The multiplicative disturbance scales with the commanded force and therefore becomes more pronounced during high-acceleration motion. In contrast, the additive disturbance induced by the gravity-compensation command persists even when the horizontal motion command is zero, leading to position-dependent steady-state force offsets.

Consequently, a feedforward controller tuned at a single operating position may achieve satisfactory local performance but can produce under-compensation or over-compensation when the mover travels to other regions. This limitation is particularly significant for long-stroke planar motion, where the mover crosses multiple spatial periods of the magnetic field. The combined effects appear as both amplitude modulation and position-dependent bias in the required control force, making them difficult to represent using a conventional linear feedforward structure with fixed parameters.

Therefore, the control problem considered in this work is to compensate for the position-dependent additive and multiplicative disturbances while preserving the nominal dynamic compensation capability of the feedforward controller. Since accurate analytical models of the magnetic-field harmonics, manufacturing deviations, and assembly errors are generally unavailable, the required spatial compensation should be learned directly from measured tracking data. Based on this consideration, a data-driven nonlinear feedforward iterative tuning method is developed in the following section.

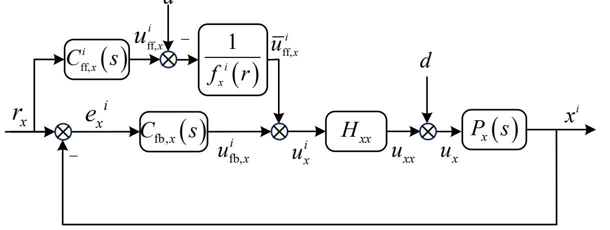

Fig. 3. Block diagram of the proposed X-DOF nonlinear feedforward control architecture

III. DESIGN OF THE PROPOSED METHOD

A. Feedforward controller parameterization

According to the feedforward branch in Fig. 3, the ideal nominal reference-trajectory feedforward signal can be parameterized as:

$$u^*_{\text{ff},x} = \boldsymbol{\lambda\theta}^* \tag{3}$$

where $\boldsymbol{\lambda}$ and $\boldsymbol{\theta}^*$ are the basis function vectors and the corresponding parameter vectors. $\mathcal{L}(\boldsymbol{\lambda\theta}^*) = P_x^{-1}(s)r_x(s)$, $\mathcal{L}(\cdot)$ is the Laplace transform.

To compensate for the additive disturbance, the compensation signal d^* is parameterized as:

$$d^* = -\boldsymbol{\gamma\vartheta}^* \tag{4}$$

where $\boldsymbol{\gamma}$ and $\boldsymbol{\vartheta}^*$ are the corresponding basis function and parameter vectors, representing the ideal additive-disturbance compensation signal.

The multiplicative disturbance compensation term can be parameterized as:

$$f_x^*(r_x) = 1 + \boldsymbol{\rho\sigma}^* \tag{5}$$

where $\boldsymbol{\rho}$ is the basis function vector, $\boldsymbol{\sigma}^*$ is the corresponding parameter vector.

The objective of the proposed feedforward controller is to generate an equivalent input that compensates both the position-dependent additive and multiplicative disturbances. For the ideal parameter set, the compensated feedforward signal should satisfy:

$$f_x^*(r_x)\bar{u}^*_{\text{ff},x} + d^* = u^*_{\text{ff},x} \tag{6}$$

Therefore, the ideal combined feedforward signal can be written as:

$$\bar{u}^*_{\text{ff},x} = \frac{u^*_{\text{ff},x} - d^*}{f_x^*(r_x)} \tag{7}$$

Substituting (3)–(5) into the above equation gives:

$$\bar{u}^*_{\text{ff},x} = \frac{\boldsymbol{\lambda\theta}^* + \boldsymbol{\gamma\vartheta}^*}{1 + \boldsymbol{\rho\sigma}^*} \tag{8}$$

Similarly, at the i-th iteration, the current parameter estimates θ^i, ϑ^i, and σ^i are used to construct the implementable feedforward signal as

$$\bar{u}^i_{\mathrm{ff},x} = \frac{u^i_{\mathrm{ff},x} - d^i}{f_x^{\,i}(r_x)} = \frac{\boldsymbol{\lambda\theta}^i + \boldsymbol{\gamma\vartheta}^i}{1 + \boldsymbol{\rho\sigma}^i} \tag{9}$$

Here, $f_x^{\,i}(r_x) = 1 + \boldsymbol{\rho\sigma}^i$ represents the estimated multiplicative gain variation, while $d^i = -\boldsymbol{\gamma\vartheta}^i$ represents the estimated additive disturbance. In this way, the numerator compensates the additive disturbance and the denominator compensates the position-dependent multiplicative disturbance.

B. Data-driven iterative feedforward tuning

Define $\boldsymbol{\delta}^i = \left[\left(\boldsymbol{\theta}^i\right)^{\mathrm{T}}, \left(\boldsymbol{\vartheta}^i\right)^{\mathrm{T}}, \left(\boldsymbol{\sigma}^i\right)^{\mathrm{T}} \right]^{\mathrm{T}}$ and $\boldsymbol{\delta}^* = \left[\left(\boldsymbol{\theta}^*\right)^{\mathrm{T}}, \left(\boldsymbol{\vartheta}^*\right)^{\mathrm{T}}, \left(\boldsymbol{\sigma}^*\right)^{\mathrm{T}} \right]^{\mathrm{T}}$, According to (9), the current feedforward signal satisfies:

$$(1 + \boldsymbol{\rho\sigma}^i)\bar{u}^i_{\mathrm{ff},x} = \boldsymbol{\lambda\theta}^i + \boldsymbol{\gamma\vartheta}^i \tag{10}$$

Thus,

$$\bar{u}^i_{\mathrm{ff},x} = \boldsymbol{\lambda\theta}^i + \boldsymbol{\gamma\vartheta}^i - \bar{u}^i_{\mathrm{ff},x}\boldsymbol{\rho\sigma}^i \tag{11}$$

For the ideal parameter set, the equivalent desired feedforward input is:

$$u^*_{\mathrm{ff},x} = f_x^{\,*}(r_x)\bar{u}^i_{\mathrm{ff},x} + d^* + \Delta u_x^{\,i} \tag{12}$$

where $\Delta u_x^{\,i}$ denotes the residual feedforward input error caused by the parameter mismatch. Therefore,

$$\Delta u_x^{\,i} = u^*_{\mathrm{ff},x} - f_x^{\,*}(r_x)\bar{u}^i_{\mathrm{ff},x} - d^* \tag{13}$$

the residual input error can be rewritten as

$$\begin{aligned} \Delta u_x^{\,i} &= \boldsymbol{\lambda}(\boldsymbol{\theta}^* - \boldsymbol{\theta}^i) + \boldsymbol{\gamma}(\boldsymbol{\vartheta}^* - \boldsymbol{\vartheta}^i) - \bar{u}^i_{\mathrm{ff},x}\boldsymbol{\rho}(\boldsymbol{\sigma}^* - \boldsymbol{\sigma}^i) \\ &= \left[\boldsymbol{\lambda}, \boldsymbol{\gamma}, -\bar{u}^i_{\mathrm{ff},x}\boldsymbol{\rho} \right](\boldsymbol{\delta}^* - \boldsymbol{\delta}^i) \end{aligned} \tag{14}$$

This equation shows that the feedforward input error is linearly parameterized with respect to the parameter error $\boldsymbol{\delta}^* - \boldsymbol{\delta}^i$.

From the closed-loop system, the tracking error caused by the residual feedforward input error $\Delta u_x^{\,i}$ can be described as:

$$e_x^{\,i}(s) = G^i(s)\Delta u_x^{\,i}(s) \tag{15}$$

For the nominal single-DOF feedback system, the plant output and the corresponding tracking error are given by:

$$x^i(s) = P_x(s)\left(\bar{u}^i_{\mathrm{ff},x}(s) + C_{\mathrm{fb},x}(s)e_x^{\,i}(s)\right) \tag{16}$$

$$e_x^{\,i}(s) = r_x(s) - x^i(s) \tag{17}$$

Let $u^*_{\mathrm{ff},x}(s) = P_x^{-1}(s)r_x(s)$ denote the ideal inverse-model feedforward input. Then the tracking error caused by the difference between $u^*_{\mathrm{ff},x}(s)$ and the actual equivalent feedforward input can be written as：

$$\begin{aligned} e_x^{\,i}(s) &= P_x(s)\Delta u_x^{\,i}(s) - P_x(s)C_{\mathrm{fb},x}(s)e_x^{\,i}(s) \\ &= \frac{P_x(s)}{1 + P_x(s)C_{\mathrm{fb},x}(s)}\Delta u_x^{\,i}(s) \end{aligned} \tag{18}$$

Since $C^i_{\mathrm{ff},x}(s)$ is designed as the nominal inverse of the plant, namely $C^i_{\mathrm{ff},x}(s) \approx P_x^{-1}(s)$,the closed-loop sensitivity can be approximated by $G^i(s) = \dfrac{1}{C^i_{\mathrm{ff},x}(s) + C_{\mathrm{fb},x}(s)}$ .Combining this relation with the parameterized residual input error gives:

$$e_x^{\,i}(s) = G^i(s)\mathcal{L}\left(\left[\boldsymbol{\lambda}, \boldsymbol{\gamma}, -\bar{u}^i_{\mathrm{ff},x}\boldsymbol{\rho} \right]\right)(\boldsymbol{\delta}^* - \boldsymbol{\delta}^i) \tag{19}$$

For implementation, the continuous-time error model is transformed into its lifted-domain representation over one trial. Let the trajectory contain N sampled data points. The lifted tracking error vector is defined as:

$$\boldsymbol{E}^i = \left[e_x^{\,i}(t_1), e_x^{\,i}(t_2), \cdots, e_x^{\,i}(t_N) \right]^T \tag{20}$$

Similarly, the filtered regressor matrix is defined as:

$$\boldsymbol{Z}^i = \left[\left(z^i(t_1)\right)^T, \left(z^i(t_2)\right)^T, \cdots, \left(z^i(t_N)\right)^T \right]^T \tag{21}$$

where

$$z^i(t) = \mathcal{L}^{-1}\left\{ G^i(s)\mathcal{L}\left(\left[\boldsymbol{\lambda}, \boldsymbol{\gamma}, -\bar{u}^i_{\mathrm{ff},x}\boldsymbol{\rho} \right]\right) \right\} \tag{22}$$

Then (19) can be written in the lifted form as:

$$\boldsymbol{E}^i = \boldsymbol{Z}^i(\boldsymbol{\delta}^* - \boldsymbol{\delta}^i) \tag{23}$$

The parameter correction can therefore be estimated by solving the least-squares problem

$$\Delta\boldsymbol{\delta}^i = \arg\min_{\Delta\boldsymbol{\delta}} \left\| \boldsymbol{E}^i - \boldsymbol{Z}^i\Delta\boldsymbol{\delta} \right\|_2^2 \tag{24}$$

The solution is

$$\Delta\boldsymbol{\delta}^i = \left((\boldsymbol{Z}^i)^T \boldsymbol{Z}^i\right)^{-1} (\boldsymbol{Z}^i)^T \boldsymbol{E}^i \tag{25}$$

Thus, the parameter vector is updated according to

$$\boldsymbol{\delta}^{i+1} = \boldsymbol{\delta}^i + \Delta\boldsymbol{\delta}^i = \boldsymbol{\delta}^i + \boldsymbol{L}^i \boldsymbol{E}^i \tag{26}$$

$$\boldsymbol{L}^i = \left((\boldsymbol{Z}^i)^T \boldsymbol{Z}^i\right)^{-1} (\boldsymbol{Z}^i)^T \tag{27}$$

This gives the data-driven iterative feedforward tuning update law. Through repeated trials, the parameter vector $\boldsymbol{\delta}^i$ is iteratively adjusted toward the ideal parameter vector $\boldsymbol{\delta}^*$, thereby reducing the tracking error caused by position-dependent additive and multiplicative disturbances.

IV. EXPERIMENTAL RESULTS

A. Experimental setup

The MLPM used in the experiments is illustrated in Fig. 4. The mover consists of 12 coils, while the stator is a two-dimensional Halbach permanent magnet array. The horizontal position is measured using laser triangulation sensors, and the vertical position is measured using eddy-current sensors. All subsequent experiments are conducted along the X-axis of the motion platform. The laser triangulation sensors have a resolution of 12 µm, and the control system operates at a sampling frequency of 5 kHz.

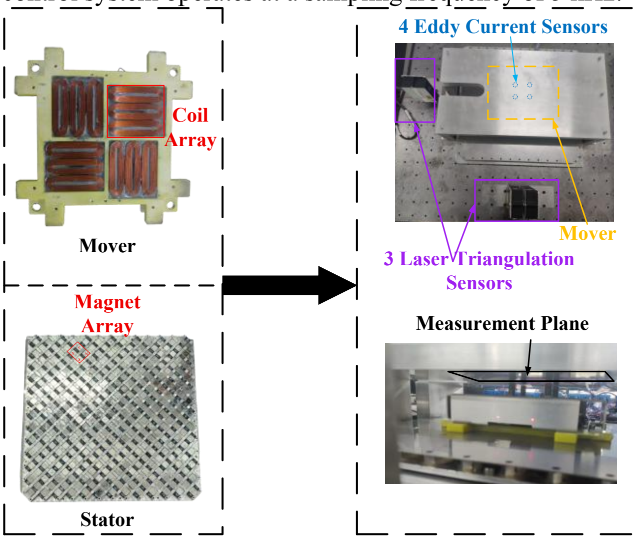

Fig. 4. MLPM used in the experiments

Fig. 5 shows the tracking error in the constant-velocity phase at a velocity of 0.1 m/s. It can be seen that due to the presence of multiplicative and additive disturbances, the error exhibits significant fluctuations. To obtain the frequency components, a fast Fourier transform (FFT) is performed on this constant-velocity phase. The results show that the dominant frequencies are at $f_n = 2.8571\text{Hz}$, thus the following basis functions are selected:

$$\boldsymbol{\rho} = \boldsymbol{\gamma} = \left[\sin(\omega_n r_x), \cos(\omega_n r_x), \sin(2\omega_n r_x),\right.$$
$$\left.\cos(2\omega_n r_x), \sin(4\omega_n r_x), \cos(4\omega_n r_x)\right]$$
$$\boldsymbol{\lambda} = [A, v]$$

where $\omega_n = 2\pi f_n / 0.1$, A and v are reference acceleration and velocity, respectively.

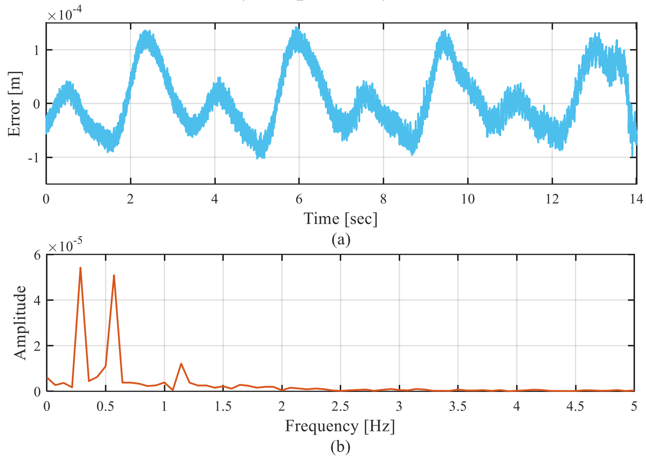

Fig. 5. (a) The error in the constant-velocity phase at 0.1 m/sec (b) The FFT of that error

A fourth-order S-curve trajectory is adopted, as shown in Fig. 6. To validate the effectiveness of the proposed method, comparisons are conducted with acceleration feedforward and combined velocity–acceleration feedforward approaches.

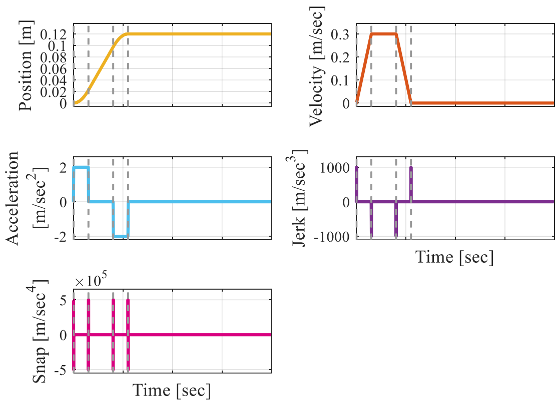

Fig. 6. Schematic diagram of the reference trajectory

B. Tracking performance

Fig. 7 shows the tracking error over iterations using the proposed method. The error decreases rapidly within the first three iterations, indicating fast initial convergence. After about five iterations, the algorithm converges, and the dynamic error over the entire stroke is significantly reduced and flattened. This demonstrates that the proposed approach can efficiently learn and compensate spatial position-dependent disturbances, greatly improving tracking accuracy. Fig. 8 compares the tracking errors of pure mass feedforward, mass–velocity feedforward, and the proposed method at the 6th iteration. Pure mass feedforward leads to large dynamic errors (over 5×10^{-4} m) due to inertia-only compensation. Mass–velocity feedforward reduces the error but still shows peaks around 0.25 s and 0.5 s because constant gains cannot handle position-dependent effects. In contrast, the proposed method significantly improves performance, with errors tightly bounded across all motion phases due to accurate compensation of spatial disturbances.

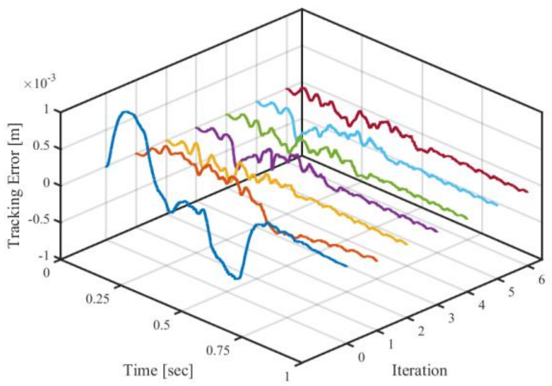

Fig. 7. Tracking errors over iterations under the proposed method

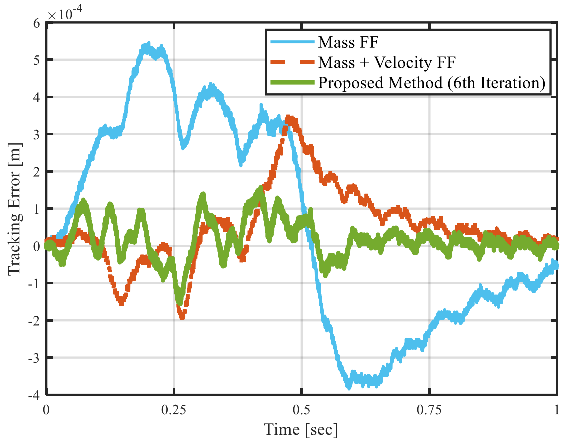

Fig. 8. Tracking errors under different methods

V. CONCLUSION

This paper presents a data-driven position-dependent rational feedforward iterative tuning strategy for MLPMs. The proposed controller compensates for both additive disturbances and multiplicative gain variations by learning parameters directly from measured errors. Experiments demonstrate convergence within six iterations and improved tracking accuracy over the full stroke.

Future work will extend the approach to full six-DOF control and investigate multi-axis high-speed coupling dynamics.

VI. ACKNOWLEDGMENTS

This work was supported in part by the National Natural Science Foundation of China under Grant 52105546, and in part by the Heilongjiang Postdoctoral Fund under Grant LBH-Z21154 and Grant LBH-TZ2314.

REFERENCES

[1] Kim, W.; Trumper, D. L.: High-precision magnetic levitation stage for photolithography, Precision Engineering, Vol. 22., No. 2., 1998, pp. 66–77.

[2] Jansen, J. W.; van Lierop, C. M. M.; Lomonova, E. A.; Vandenput, A. J. A.: Modeling of magnetically levitated planar actuators with moving magnets, IEEE Transactions on Magnetics, Vol. 43., No. 1., 2007, pp. 15–25.

[3] Ou, T.; Hu, C.; Zhu, Y.; Zhang, M.: Generation mechanism and decoupling strategy of coupling effect in maglev planar motor, IEEE/ASME Transactions on Mechatronics, Vol. 28., No. 2., 2023, pp. 781–791.

[4] Broens, Y.; Butler, R.: On improved commutation for moving-magnet planar actuators, IEEE Control Systems Letters, Vol. 7., 2023, pp. 2593–2598.

[5] Rovers, J. M. M.; Jansen, J. W.; Lomonova, E. A.: Multiphysical analysis of moving-magnet planar motor topologies, IET Electric Power Applications, Vol. 7., No. 1., 2013, pp. 42–50.

[6] Heertjes, M.; Hennekens, D.; Steinbuch, M.: MIMO feed-forward design in wafer scanners using a gradient approximation-based algorithm, Control Engineering Practice, Vol. 18., No. 5., 2010, pp. 495–506.

[7] Bristow, D. A.; Tharayil, M.; Alleyne, A. G.: A survey of iterative learning control, IEEE Control Systems Magazine, Vol. 26., No. 3., 2006, pp. 96–114.

[8] Blanken, L.; Oomen, T.: Multivariable iterative learning control design procedures: From decentralized to centralized, illustrated on an industrial printer, IEEE Transactions on Control Systems Technology, Vol. 28., No. 4., 2020, pp. 1534–1541.

[9] Jiang, Y.; Zhu, Y.; Yang, K.; Hu, C.; et al.: A data-driven iterative decoupling feedforward control strategy with application to an ultraprecision motion stage, IEEE Transactions on Industrial Electronics, Vol. 62., No. 1., 2015, pp. 620–627.

[10] Li, M.; Mao, C.; Zhu, Y.; Yang, K.; et al.: Data-based iterative dynamic decoupling control for precision MIMO motion systems, IEEE Transactions on Industrial Informatics, Vol. 16., No. 3., 2020, pp. 1668–1676.

[11] de Rozario, R.; Oomen, T.; Steinbuch, M.: Iterative learning control and feedforward for LPV systems: Applied to a position-dependent motion system, Proceedings of the American Control Conference (ACC), 2017, pp. 3518–3523.